WELL PRODUCTION WITH CASING SAND BRIDGE

Doru Stoianovici [1]

Timur Chis [1]

[1] Petroleum-Gas University of Ploiesti, Romania
email: doru.stoianovici@yahoo.com

DOI: 10.51865/JPGT.2023.01.09

ABSTRACT

Many reservoirs comprised of relatively young sediments are so poorly consolidated that sand will be produced along with the reservoir fluids unless the rate is restricted significantly. The mathematical modelling of the flow of the sanded well uses the continuity equation written in cylindrical coordinates, Darcy's law admitting its availability and the solutions of these equations obtained for the boundary conditions in the case of a crude oil well that produces sand floods.

In this article we have created a numerical model based on the variation of fluid flow from the productive layer, depending on the pressure drop between the productive layer and the wellbore, as well as the permeability of the layer. As a function of the flows extracted from the well, we rewrote the flow variation equations as polynomial relations of order 5, the error being a maximum of 0.04%. After determining the flow through the two relationships and confronting the reality in the field, the article confirms the type of flow through sand.

Keywords: sand, sand control, oil extraction, casing sand bridge

1. INTRODUCTION

To analyse the performance of the production system is used a system analysis approach, also known as *Nodal Analysis*.

This method was initially proposed by Gilbert in 1954 and further developed by Ning in 1964 and Brown in 1978 [1,2,3].

The system analysis consists of selecting a node (point) in the well and divide the production system at this point.

The most common nodes are separator, surface choke, wellhead, safety valve, diameter restriction (in the tubulars), bottom hole (in the well), at sand face and in the reservoir.

At a specific moment in the lifetime of the well, the average reservoir pressure and the system outlet pressure are only two pressures that always remain fixed and are not function of the flowrate.

The outlet pressure can be the separator pressure or the wellhead pressure, if the well is controlled by a surface choke.

Once the node has been chosen, the node pressure is calculated from both directions, starting at the fixed pressures.

A series of flowrate is used to calculate node pressures for each section of the system, then are made plots of node pressure vs production rate for the inflow and outflow section.

The curve representing the inflow section is called the inflow curve, while the curve representing the outflow section is the outflow curve.

The intersection of the two curves provides the point of continuity required by the systems analysis approach and indicates the anticipated production rate and pressure for the analysed system [5, 6].

To carry out the study, the use of *nodal analysis* by the side of equation writing, applied to a crude oil well that produced in the first stage with free perforations; during exploitation, due to the weakly consolidated productive layer, the sand rose in the column, over the entire thickness of the productive layer.

2. MATHERIALS AND METHODS

2.1. Mathematical modelling of the sanded well flow rate

If the productive layer consists of poorly consolidated sand, there is a possibility that the crude oil will enter the well together with the sand particles.

In the well, the upward fluid flow drives the lighter sand grains to the surface, while the heavier sand grains are deposited at the bottom of the well and form a layer of sand whose height may exceed the thickness of the productive layer [1].

It is considered a sandy well, which produces from an area of cylindrical shape and permeability k_2; the permeability of the sand in the well is k_1, and its height is considered equal to the thickness h of the productive layer. The configuration of the movement (fig.1) highlights the axially symmetrical character of the movement [1,2,3].

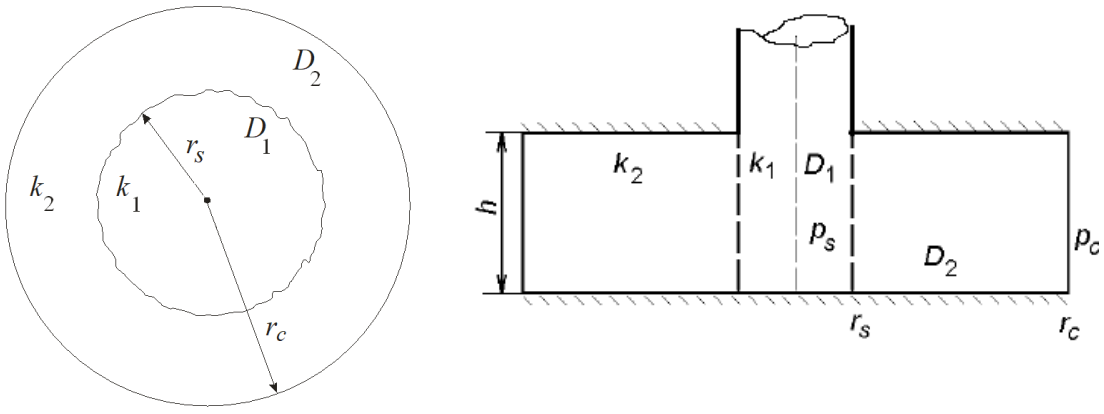

Figure 1. Radial flow for well casing sand bridge [1,11]

Noting with D_1 the domain $0 \le r \le r_s$; $0 \le z \le h$ and with D_2 area $r_s \le r \le r_c$; $0 \le z \le h$, and associating indices 1 to the movement parameters in D_1 and 2 to the movement parameters in D_2, the movement equations, related to the cylindrical coordinate axes, are presented as follows [2,3,4]:

$$v_{ri} = -\frac{k_i}{\mu}\frac{\partial p_i}{\partial r} \tag{1}$$

$$v_{zi} = -\frac{k_i}{\mu}\frac{\partial p_i}{\partial z} \tag{2}$$

from Darcy's low and [3,5]

$$\frac{1}{r}\frac{\partial}{\partial r}(r\rho v_r) + \frac{\partial}{\partial z}(\rho v_z) = 0 \tag{3}$$

from continuity equation in cylindrical coordinates written for an incompressible liquid, homogeneous porous medium and steady state conditions [5,6,7].

Eliminating the velocity components, from equations (1), (2) and (3) the differential pressure equation is obtained [8,9,10]:

$$\frac{1}{r}\frac{\partial}{\partial r}\left(r\frac{\partial p_i}{\partial r}\right) + \frac{\partial^2 p_i}{\partial z^2} = 0 \quad \text{(i=1;2)} \tag{4}$$

whose solutions must satisfy the following boundary conditions:

$$v_{z1} = -\frac{k_1}{\mu}\frac{\partial p_1}{\partial z} = \begin{cases} 0; \ z = 0, 0 \le r \le r_s \\ \frac{Q}{\pi r_s^2}; z = h, \ 0 \le r \le r_s \end{cases} \tag{5}$$

$$v_{z2} = -\frac{k_2}{\mu}\frac{\partial p_2}{\partial z} = 0 \begin{cases} z = 0, \ r_s \le r \le r_c \\ z = h, \ r_s \le r \le r_c \end{cases} \tag{6}$$

$$p_1 = p_2 \ ; \quad r = r_s \ ; \quad 0 \le z \le h \quad \text{(at the borehole wall)} \tag{7}$$

$$k_1\frac{\partial p_1}{\partial r} = k_2\frac{\partial p_2}{\partial r}; \quad \text{if} \quad r = r_s \quad \text{and} \quad 0 \le z \le h \tag{8}$$

$$p_2 = p_c \ ; \quad r = r_c \ ; \quad 0 \le z \le h \tag{9}$$

$$p_1 = p_{s0} \ ; \quad r = 0 \ ; \quad z = h \tag{10}$$

$$p = \begin{cases} p_1, \ 0 \le r \le r_s \ , 0 \le z \le h \\ p_2, \ r_s \le r \le r_c \ , \ 0 \le z \le h \end{cases} \tag{11}$$

The differential equations (4) accepts solutions of the form:

$$p_+ = R(r) + Z(z) \tag{12}$$

Replacing solution (12) in the equation: $\frac{1}{r}\frac{\partial}{\partial r}\left(r\frac{\partial p}{\partial r}\right) + \frac{\partial^2 p}{\partial z^2} = 0$, result:

$$\frac{1}{r}\frac{d}{dr}\left(r\frac{dR}{dr}\right) + \frac{d^2 Z}{dz^2} = 0 \tag{13}$$

which is equivalent to the system:

$$-\frac{1}{r}\frac{d}{dr}\left(r\frac{dR}{dr}\right) = \frac{d^2 Z}{dz^2} = A \tag{14}$$

whose integration leads to the relations:

$$Z = A\frac{z^2}{2} + Bz + C \tag{15}$$

$$R = -A\frac{r^2}{4} + D\ln r + E \tag{16}$$

therefore, solution (12) is of the form:

$$p_+ = \frac{A}{2}\left(z^2 - \frac{r^2}{2}\right) + Bz + D\ln r + C + E \tag{17}$$

But the equation $\frac{1}{r}\frac{\partial}{\partial r}\left(r\frac{\partial p}{\partial r}\right) + \frac{\partial^2 p}{\partial z^2} = 0$ also accepts a general solution of the form:

$$p = R(r)\cdot Z(z) \tag{18}$$

Thus, the differential pressure equation becomes:

$$Z\frac{d^2R}{dr^2} + \frac{Z}{r}\frac{dR}{dr} + R\frac{d^2Z}{dz^2} = 0 \tag{19}$$

which is equivalent to the equations:

$$\frac{1}{R}\frac{d^2R}{dr^2} + \frac{1}{rR}\frac{dR}{dr} = -\frac{1}{Z}\frac{d^2Z}{dz^2} = s^2 \tag{20}$$

which can also be written in the form:

$$r^2\frac{d^2R}{dr^2} + r\frac{dR}{dr} - s^2r^2R = 0 \tag{21}$$

$$\frac{d^2Z}{dz^2} + s^2Z = 0 \tag{22}$$

Equation (21) is a transformed Bessel equation with the general solution:

$$R = AI_0(sr) + BK_0(sr) \tag{23}$$

with *A* and *B* is constant and I_0 and K_0 are modified Bassel functions of the First and Second Kind and of zero order [2,3,4] (fig.1).

Equation (22) has the solution:

$$Z = C\cos sz + D\sin sz \tag{24}$$

Therefore, equation (4) also accepts a solution of the form:

$$p = C_0 + B_0\ln r + \sum_{n=1}^{\infty}\left(a_n\cos\frac{\pi nz}{h} + b_n\sin\frac{\pi nz}{h}\right)I_0\left(\frac{\pi nr}{h}\right) +$$

$$+\sum_{n=1}^{\infty}\left(c_n\cos\frac{\pi nz}{h} + d_n\sin\frac{\pi nz}{h}\right)K_0\left(\frac{\pi nr}{h}\right) \tag{25}$$

The linear combination of solutions (17) and (23):

$$p = a + b\ln r + c\left(z^2 - \frac{r^2}{2}\right) + dz + \sum_{n=1}^{\infty}\left(a_n\cos\frac{\pi nz}{h} + b_n\sin\frac{\pi nz}{h}\right)I_0\left(\frac{\pi nr}{h}\right) +$$

$$+\sum_{n=1}^{\infty}\left(c_n\cos\frac{\pi nz}{h} + d_n\sin\frac{\pi nz}{h}\right)K_0\left(\frac{\pi nr}{h}\right) \tag{26}$$

it's a solution that meets the conditions imposed [6,7].

Imposing on solution (22) the conditions (5) and (6), it turns out that $d=b_n=d_n=0$ (fig.1). Since $r \to 0$, $k_0(r) \to \infty$ and $\ln r \to -\infty$ and at large values of the radius $I_0(r)$ is negligible, p function reduces to [8,9,10]:

$$p = \begin{cases} p = a^* + c\left(z^2 - \frac{r^2}{2}\right) + \sum_{n=1}^{\infty} a_n I_0\left(\frac{\pi n r}{h}\right)\cos\frac{\pi n z}{h}, & 0 \le r \le r_s,\ 0 \le z \le h \\ p = a + b\ln r + \sum_{n=1}^{\infty} c_n K_0\left(\frac{\pi n r}{h}\right)\cos\frac{\pi n z}{h}, & r_s \le r \le r_c,\quad 0 \le z \le h \end{cases} \tag{27}$$

From conditions (5) to (10) imposed on solution (27), result [8,9,10]:

1) $\left(\frac{\partial p_1}{\partial z}\right)_{(z=h)} = -\frac{\mu Q}{\pi r_s^2 k_1} = 2hc;$

2) $a + c\left(z^2 - \frac{r^2}{2}\right) + \sum_{n=1}^{\infty} a_n I_0\left(\frac{\pi n r}{h}\right)\cos\frac{\pi n z}{h} = a + b\ln r_s + \sum_{n=1}^{\infty} c_n K_0\left(\frac{\pi n r}{h}\right)\cos\frac{\pi n z}{h};$

3) $-cr_s + \frac{\pi}{h}\sum_{n=1}^{\infty} n a_n I_1\left(\frac{\pi n r}{h}\right)\cos\frac{\pi n z}{h} = \frac{k_2}{k_1}\left[\frac{b}{r_s} - \frac{\pi}{h}\sum_{n=1}^{\infty} n c_n K_1\left(\frac{\pi n r}{h}\right)\cos\frac{\pi n z}{h}\right];$

4) $p_c = a + b\ln r_c;$

5) $p_{s0} = a^* + h^2 c + \sum_{n=1}^{\infty}(-1)^n a^n.$

It is taken into account that: $I_0(0) = 0$ and $K_0\left(\frac{\pi n r}{h}\right) \cong 0$ [12,13].

The second and third relations can be written in the form:

2') $-a^* + b\ln r_s - c\left(z^2 - \frac{r^2}{2}\right) = \sum_{n=1}^{\infty}\left[a_n I_0\left(\frac{\pi n r}{h}\right) - c_n K_0\left(\frac{\pi n r}{h}\right)\right]\cos\frac{\pi n z}{h};$

3') $r_s + \frac{\delta}{r_s}b = \frac{\pi}{h}\sum_{n=1}^{\infty}\left[n a_n I_1\left(\frac{\pi n r}{h}\right) + \delta c_n K_1\left(\frac{\pi n r}{h}\right)\right]\cos\frac{\pi n z}{h};$

where the terms on the right are Fourier series, $\delta = \frac{K_2}{K_1}$, and functions $f_1(z) = a - a^* + b\ln r_s - c\left(z^2 - \frac{r^2}{2}\right)$ and $f_2 = cr_s + \frac{\delta}{r_s}b$ are according to (2') and (3') the even periodic functions, with period $\omega = \frac{\pi}{h}$ and pulsation $T = \frac{2\pi}{\omega} = 2h$ and have the Fourier coefficients given by the relations:

$$A_n = a_n I_0\left(\frac{\pi n r}{h}\right) - c_n K_0\left(\frac{\pi n r}{h}\right) = \frac{2}{h}\int_0^h f_1(z)\cos\frac{\pi n z}{h}\,dz = -\frac{4h^2 c(-1)^n}{n^2\pi^2} \tag{28}$$

$$C_n = \frac{\pi}{h}n\left[a_n I_1\left(\frac{\pi n r}{h}\right) + \delta c_n K_1\left(\frac{\pi n r}{h}\right)\right] = \frac{2}{h}\int_0^h f_2\cos\frac{\pi n z}{h}\,dz = 0 \tag{29}$$

$$A_0 = \frac{1}{h}\int_0^h f_1(z)\,dz = a - a^* + b\ln r_s - c\left(\frac{h^2}{3} - \frac{r_s^2}{2}\right) = 0 \tag{30}$$

$$C_0 = \frac{1}{h}\int_0^h f_2\,dz = cr_s + \frac{\delta}{r_s}b = 0 \tag{31}$$

from the first two equations [14,15]:

$$a_n = -\frac{4h^2 c(-1)^n}{n^2\pi^2\left[I_0\left(\frac{\pi n r_s}{h}\right) + \frac{I_1\left(\frac{\pi n r_s}{h}\right)K_0\left(\frac{\pi n r_s}{h}\right)}{\delta K_1\left(\frac{\pi n r_s}{h}\right)}\right]} \tag{32}$$

$$c_n = -\frac{I_1\left(\frac{\pi n r_s}{h}\right)}{\delta K_1\left(\frac{\pi n r_s}{h}\right)} a_n; \quad n = 1, 2, 3, \ldots \tag{33}$$

the relations A_0 and C_0 solved according to a, a^*, b and c give the following expressions of the integration constants:

$$a = p_c - \frac{p_c - p_{s0} + \sum_{n=1}^{\infty}(-1)^n a_n}{\ln\frac{r_c}{r_s} + \delta\left(\frac{2h^2}{3r_s^2} + \frac{1}{2}\right)} \ln r_c \tag{34}$$

$$a^* = p_{s0} + \delta\frac{h^2}{r_c^2} \cdot \frac{p_c - p_{s0} + \sum_{n=1}^{\infty}(-1)^n a_n}{\ln\frac{r_c}{r_s} + \delta\left(\frac{2h^2}{3r_s^2} + \frac{1}{2}\right)} - \sum_{n=1}^{\infty}(-1)^n a_n \tag{35}$$

$$b = \frac{p_c - p_{s0} + \sum_{n=1}^{\infty}(-1)^n a_n}{\ln\frac{r_c}{r_s} + \delta\left(\frac{2h^2}{3r_s^2} + \frac{1}{2}\right)} \tag{36}$$

$$c = -\frac{\delta}{r_s^2} \cdot \frac{p_c - p_{s0} + \sum_{n=1}^{\infty}(-1)^n a_n}{\ln\frac{r_c}{r_s} + \delta\left(\frac{2h^2}{3r_s^2} + \frac{1}{2}\right)} \tag{37}$$

replacing the constant a_n from equation (37) with expression (32), constant c from equation (37) take form:

$$c = -\frac{p_c - p_{s0}}{\frac{\delta}{r_s^2}\ln\frac{r_c}{r_s} + \frac{2}{3}h^2 + \frac{r_s^2}{2} - \frac{4h^2}{\pi^2}\sum_{n=1}^{\infty} H_n} \tag{38}$$

where,

$$H_n = \frac{1}{n^2\left[I_0\left(\frac{\pi n r_s}{h}\right) + \frac{I_1\left(\frac{\pi n r_s}{h}\right)K_0\left(\frac{\pi n r_s}{h}\right)}{\delta K_1\left(\frac{\pi n r_s}{h}\right)}\right]} \tag{39}$$

results the flow rate of the well with casing sand bridge [1,2,11]:

$$Q = \frac{2\pi k_1 h(p_c - p_{s0})}{\mu\left(\frac{1}{\delta}\ln\frac{r_c}{r_s} + \frac{2h^2}{3r_s^2} + \frac{1}{2} - \frac{4h^2}{\pi^2 r_s^2}\sum_{n=1}^{\infty} H_n\right)} \tag{40}$$

The imperfection coefficient witch is the ratio between the flow rate of the sanded well and that of the perfect well is given by the relation:

$$\frac{Q}{Q_0} = \frac{\ln\frac{r_c}{r_s}}{\delta\left(\frac{1}{\delta}\ln\frac{r_c}{r_s} + \frac{2h^2}{3r_s^2} + \frac{1}{2} - \frac{4h^2}{\pi^2 r_s^2}\sum_{n=1}^{\infty} H_n\right)} \tag{41}$$

Where Q_0 is the free perforated well flow rate and $= \frac{K_2}{K_1}$.

2.2. Comparative analysis of the sanded well flow rate and the free perforated well flow rate

2.2.1. Case study

The influence of the sand bridge in the well casing was analysed for a well whose data are presented in table 1, for the permeability of the layer K_2 = 50 mD and for the permeability of the sand bridge K_1=100 mD, 200 mD, 300 mD respectively 500 mD. (Figures 2, 3, 4)

From the production data of the well, it is observed that the flow is greatly reduced even when the sand bridge permeability is much higher than the permeability of the layer.

Thus, for $K_1=2K_2$, the well flow decrease to 10.8 % and if $K_1=10K_2$, the well flow decrease to 38.2 %.

This behaviour of the sanded well can also be observed from the variation graph of the imperfection coefficient.

The relationships and numerical examples presented in the work highlighted the need to avoid the well exploitation in the presence of sand bridge in the well casing.

Table 1. Well data

Reservoir pressure	190	bar	Perforation density	11	SPM
Reservoir permeability (K_2)	50	mD	Perforation diameter	43	mm
Reservoir thickness	22	m	Damaged zone permeability	2	mD
Perforation interval	22	m	Damaged zone radius	650	mm
Reservoir temperature	56	ºC	Perm ratio kc / kf	0.7	
Reservoir temperature	55	ºC	Wellbore radius	220	mm
Reservoir area	488	ha	Casing diameter	5,5	in
Water density	1070	kg/m^3	Tubing diameter	2.875	in
Oil density	830	kg/m^3	Flow line length	1500	m
Water cut	30	%	Flow line diameter	66.65	mm
Gas oil ratio	388	m^3(g)/m^3(l)	Separator pressure	8	bar

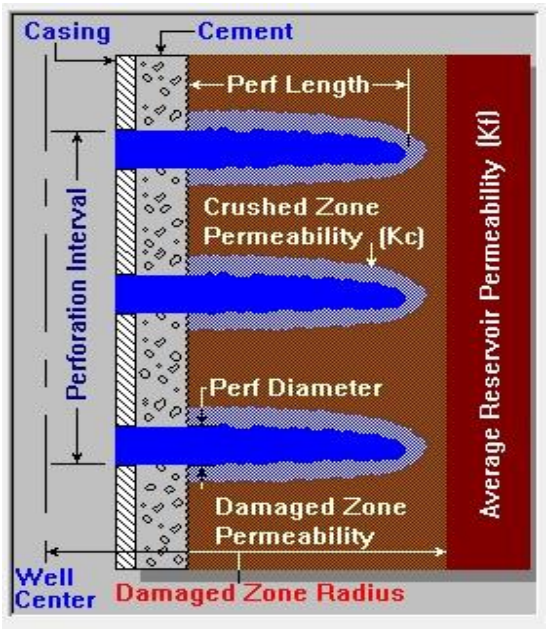

Figure 2(a). Well completion without casing sand bridge

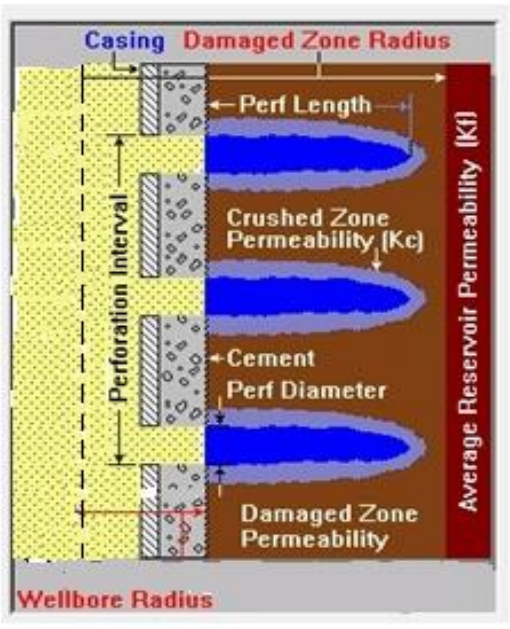

Figure 2(b). Well completion with casing sand bridge

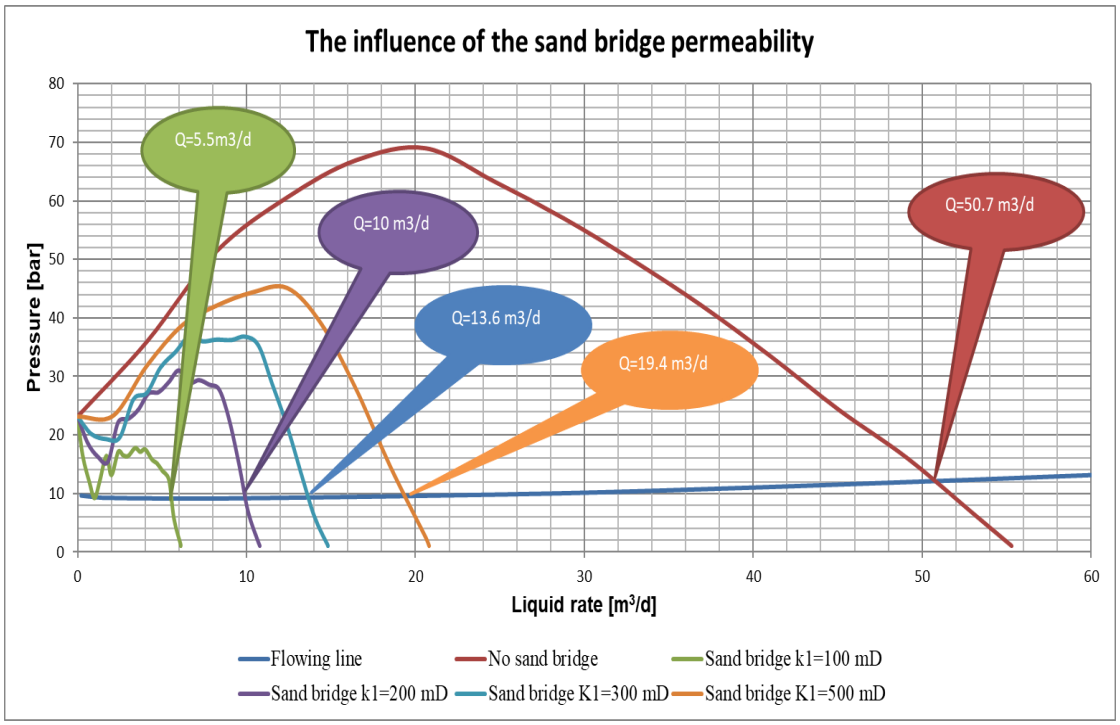

Figure 3. The influence of sand bridge permeability on well flow

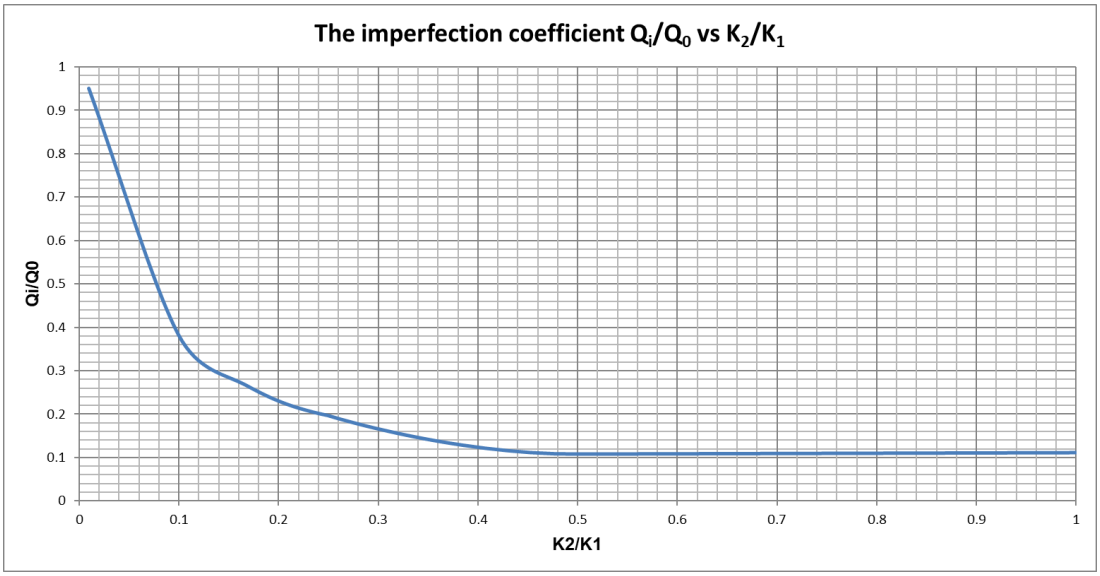

Figure 4. The imperfection coefficient depending on sand bridge permeability and layer permeability

2.2.2. Input Data and Simulation Results

To observe the effect of the sand bed (sand filter) on the production of a crude oil well, we used nodal sensitivity analysis, which included in the study the measurable components of a production well from a productive layer of crude oil located in a field with a pressure of 190 bar.

We studied the effect of the fluid flow rate on the pressure drop in the productive layer (when the fluid passes through sand with various permeabilities).

The analyzes were carried out with the help of relation 41 and confirmed with the PIPESIM, software that best describes these transient phenomena in the area of productive wells (figure 3 and Table 2).

Table 2. Simulation results for the well production data

No casing sand bridge		Sand bridge permeability K_1=100mD		Sand bridge permeability K_1=200mD		Sand bridge permeability K_1=300mD		Sand bridge permeability K_1=500mD		Flowing line	
Liquid rate	Press.	Liquid rate	Press.	Liquid rate	Press.	Liquid rate	Press.	Liquid rate	Press.	Liquid rate	Press.
m^3/d	bar	m^3/d	bar	m^3/d	bar	m^3/d	bar	m^3/d	bar	m^3/d	bar
0	23.15	0	23.15	0	23.15	0	23.15	0	23.15	0.2	9.6
4.1	35.95	0.3	16.47	0.6	18.6	0.8	20.17	2.1	23.28	1.3	9.26
8.2	51.34	0.7	11.88	1.2	16.26	1.7	19.27	4.1	31.84	2.0	9.2
12.4	60.63	1.0	9.19	1.8	15.41	2.5	19.59	6.2	38.79	2.7	9.16
16.5	67.02	1.3	12.02	2.4	22.14	3.3	26.07	8.2	42.09	3.6	9.13
20.6	69.05	1.7	16.42	3.0	22.74	4.1	27.18	10.3	44.35	4.7	9.11
24.7	63.32	2.0	13.14	3.6	24.31	4.9	31.51	12.4	45.14	6.1	9.09
28.8	57.03	2.4	17.12	4.2	27.07	5.8	34.21	14.4	39.09	8.0	9.09
32.8	50.02	2.7	16.51	4.8	27.3	6.6	36.85	16.5	27.69	11.4	9.19
36.9	42.22	3.0	16.44	5.4	29.0	7.4	36.0	18.5	14.59	20.5	9.56
41.0	33.52	3.4	17.77	6.0	31.02	8.2	36.29	20.6	2.44	30.4	10.12
45.1	24.22	3.7	17.12	6.6	28.88	9.1	36.22	20.8	1.01	41.8	11.15
49.1	16.07	4.0	17.53	7.2	29.36	9.9	36.79			53.2	12.33
53.2	6.12	4.4	15.8	7.8	28.58	10.7	35.25			64.6	13.63
55.3	1.01	4.7	15.14	8.4	27.7	11.5	28.76			76.0	15.03
		5.0	13.91	9.0	22.42	12.4	21.4				
		5.4	12.32	9.6	14.47	13.2	13.56				
		5.7	5.6	10.1	6.91	14.0	6.05				
		6.1	1.2	10.7	1.73	14.8	1.08				
		6.1	1.01	10.8	1.01	14.8	1.01				
Q =50.7 m^3/d		**Q =5.5 m^3/d**		**Q =10 m^3/d**		**Q =13.6 m^3/d**		**Q =19.4 m^3/d**			

The role of this sensitivity analysis is to establish the evolution of the flow according to various permeabilities and especially the problems that may arise (in the case of an increase in the inflow of sand into the well).

Also, the imperfection coefficient Q_i/Q_0 can be represented depending on the permeability ratio k_2/k_1 (Figure 4).

3. DISSCUSION

The analysis of the influence of the permeability of the productive layers showed the reduction of fluid flow from 50.7 mc/d to 5.5 mc/d, depending on the type of sand filter located in the production area. Also, the simulation showed us the possibility of using polynomial relations of the 6th degree that provide in real time the flow rate of the well as a function of the pressure of the productive layer x is Liquid rate (mc/d) and y is pressure (bar):

Productive layers	Equation	R^2
No casing sand bridge	$y = 5E\text{-}08x^6 - 1E\text{-}05x^5 + 0.0008x^4 - 0.0268x^3 + 0.2848x^2 + 2.416x + 23.131$	0.9993
Sand bridge permeability K_1=100mD	$y = 0.0194x^6 - 0.4397x^5 + 3.8693x^4 - 16.965x^3 + 37.931x^2 - 36.823x + 23.59$	0.9609
Sand bridge permeability K_1=200mD	$y = 0.0017x^6 - 0.0576x^5 + 0.7405x^4 - 4.6793x^3 + 14.916x^2 - 18.681x + 23.794$	0.9847
Sand bridge permeability K_1=300mD	$y = 0.0002x^6 - 0.0108x^5 + 0.1848x^4 - 1.5983x^3 + 7.0707x^2 - 11.019x + 23.787$	0.9927
Sand bridge permeability K_1=500mD	$y = 3E\text{-}05x^6 - 0.0018x^5 + 0.0418x^4 - 0.4995x^3 + 2.8936x^2 - 3.8709x + 23.035$	0.9983
Flowing line	$y = 9E\text{-}10x^6 - 2E\text{-}07x^5 + 2E\text{-}05x^4 - 0.0008x^3 + 0.0183x^2 - 0.1592x + 9.5133$	0.9993

The objectives of this work is to quantify the effect of the pressure drop on the flow produced by a well affected by the productive sand layers.

The sensitivity of the permeability of the sand layer was analyzed by nodal analysis and it was found that in a productive well, difficulties may arise in ensuring the flow with more than 90% of the initial flow (at a reduced permeability).

The simulations carried out allow the probe to be followed in production, the three models chosen in this article (numerical calculation, simulation using the PIPESIM software and especially the algebraic equations of ordinal 6) confirm the reality in the field with an approximation of 0.06% (in the case of numerical equations) and of 0.055 % in the case of the PIPESIM software.

Most researchers perform wellbore simulation only for flow in surface conduits and production tubing and less in productive strata (since flow problems can occur in these areas). But in order to determine the optimal period for cracking the productive layers, such an analysis is useful.

4. CONCLUSIONS

Thus, for a well that exploits a productive karst (without sand), upon commissioning we have an increase in pressure (which is due to the start of the productive layer) followed by an increase in flow rate with a decrease in pressure.

The objectives of the paper were to analyze which of the three numerical models best describes the flow of petroleum fluids through sand beds.

Thus we concluded that the PIPESIM software is the easiest to use, but to simulate the production of the layers, numerical equations of the 6th order can also be created.

The article considered nodal analysis of the production of an oil well possibly affected by sand floods in the future.

It resulted in a simulation of the pressure drop depending on the extracted flow rate and especially the possibility to determine the porosity of the productive layers.

In addition to the numerical model proposed by us, it is recommended to use software analysis, which is simple to use.

REFERENCES

[1] Damascan, A., Albulescu, M., Chis, T., The Mathematical Modeling of the Flow Variation of Natural Gas Extraction Wells Depending on the Diameter of the Mixing Pipe, Engineering and Technology Journal, Vol.7, Issue 9, 2022, pp. 1477-1482, http://everant.org/index.php/etj/article/view/701.

[2] Damascan A., Albulescu M., Stoianovici D., The Influence of the Perforation Density and Damaged Zone Permeability on a Gas Well Production, Romanian Journal of Petroleum & Gas Technology Vol. 3 (74), No. 2/2022, pp. 65-76, DOI: 10.51865/JPGT.2022.02.07.

[3] Ngankam R.M.K., Dongmo E.D., Nitcheu M., Matateyou J.F., Kuiatse G., Kingni S.T., Production Step-Up of an Oil Well through Nodal Analysis, Journal of Engineering, vol. 2022, Article ID 6148337, https://doi.org/10.1155/2022/6148337.

[4] Sorrell S., Speirs J., Bentley R., Miller R., Thompson E., Shaping the global oil peak: a review of the evidence on field sizes, reserve growth, decline rates and depletion rates, Energy, vol. 37, no. 1, pp. 709–724, 2012.

[5] Matateyou J.F., Njeudjang K., Donald Dongmo E., Rengou Mbouombouo C.I., Kamnang Konchipe H.V., Kuiatse G., Design of continuous gas-lift for a dead well and step-up of its productivity, Petrovietnam Journal, vol. 6, pp. 43–48, 2022.

[6] Gao J., Yao Y., Wang D., Tong H., A comprehensive model for simulating supercritical-water flow in a vertical heavy-oil well, SPE Journal, vol. 26, no. 06, pp. 4051–4066, 2021.

[7] Stoianovici G., Stoianovici D., Nicolescu C., Effect of Sand Control Techniques on Oil Well Performance, Petroleum-Gas University of Ploieşti Bulletin, Vol. LXVII, No.4/2015.

[8] Stoianovici D., Stoicescu M., Dynamics of fluids through porous media, Petroleum-Gas University of Ploieşti Publishing House, 2019.

[9] Brown, K.E., James, F.L., Nodal Systems Analysis of Oil and Gas Wells, JPT. Vol. 37, October 1985.

[10] Beggs, H.D., Production Optimization Using Nodal Analysis, SPE, Richardson, TX, 2003.

[11] Dinu, F., Natural gas extraction, Petroleum-Gas University of Ploieşti Publishing House, 2000.

[12] Dmour, H.D., Optimization of Well Production System by NODAL Analysis Technique, Petroleum Science and Technology, Vol. 31, Issue 11, June 2013, pp. 1109-1122.

[13] Karakas, M., and Tariq, S., Semi-Analytical Production Models for Perforated Completions, SPE Paper 18247, 1988.

[14] Krueger, R.F., An Overview of Formation Damage and Well Productivity in Oilfield Operations, JPT 131 – 152, February 1986.

[15] Stoianovici D., Stan Al.D., Profitability of a well in crude oil pumping with sand floods, Mine, Petrol, Gaze, 1990.

Received: February 2023; Accepted: February 2023; Published: February 2023